

Galaxy Dynamics and their Dark Matter Content

Honours Project

Nhlakanipho Sabelo Kunene



Physics and Astronomy Department
University of the Western Cape

Supervisor: Dr. L Lerothodi
Co-Supervisor: Dr. G Sharma

Contents

1 Overview	3
2 Introduction	3
2.1 Type of Galaxies	3
2.1.1 Spiral galaxy	4
2.1.2 Elliptical galaxies:	5
2.1.3 Irregular galaxies	6
2.1.4 Dwarf galaxies	6
2.2 Various Galaxy Components	7
2.2.1 Dark Matter Halo	7
2.2.2 Globular cluster	7
2.2.3 Stellar disk	8
2.2.4 Gas Disk	8
2.2.5 Stellar Bulge	9
2.2.6 Black hole	9
2.3 Summary	10
3 Galaxy Kinematics	11
3.1 Observations	11
3.1.1 Conventional Spectroscopy	11
3.1.2 Integral Field Spectroscopy	14
3.2 Data	16
3.3 Barolo	17
3.3.1 3D Barolo installation	18
3.3.2 Barolo Inputs	20
3.3.3 Barolo Outputs	22
4 Galaxy Dynamics	26
4.1 Stellar Disk	26
4.2 Gas disk	27
4.3 Stellar bulge	27
4.4 Halo	29
4.4.1 Cuspy Dark Matter Halo	29
4.4.2 Cored Dark Matter Halo	30
4.5 Modelling a mock rotation curve	30
5 Results	32
5.1 Testing Barolo	32
5.1.1 Position Angle	32
5.1.2 Inclination Angle	34
5.1.3 Systematic Velocity	36
5.2 Dark Matter Fractions of NGC2403	38

6 Conclusion

41

1 Overview

Dark matter makes 27% of energy budget in the Universe. However, nature of dark matter remains a mystery. In the late 1970s, using galaxy dynamics Vera Rubin showed that flat circular velocity profiles are ubiquitous in local galaxies. Based on this, she concluded that “galaxies are surrounded by an invisible matter, the so-called dark matter halo, that extends much farther than their visible matter”. In this project we will learn about this mysterious dark matter halo and its properties in the local Universe.

This project is aimed to teach the chronological history of dark matter, galaxy dynamics, and determination of dark matter content in galaxies (theoretical+observational). We will use tools such as python, matplotlib, and topcat for reading, writing, and visualizing the datasets. In particular, we pick-up a local galaxy named NGC2403, and determine its dark matter content using robust techniques.

2 Introduction

Galaxies are some of the most beautiful and fascinating objects in the Universe. Galaxies are in different shapes and morphology, this is due to evolution. Galaxy contain different masses that describes how much angular momentum there is that also helps us in making structure. They come in a large variety of sizes and shapes, colors and brightness. In this section below we will classify galaxies in accordance to their observed properties into their types.

2.1 Type of Galaxies

Galaxies are classified in terms of the Hubble Sequence, a morphological classification scheme for galaxies invented by Edwin Hubble in 1926. Edwin Hubble [5] first discovered an evolutionary sequence of galaxies as the tuning fork. Hubble arranged galaxies into the tuning-fork diagram and categorized them into three groups based on their appearance, i.e., ellipticals (E's),spirals (S's) and irregulars (Irr's). Spirals are further divided into two separated sequences, the normal spirals without bars (S's) and the barred spirals (SB's). A transition type between ellipticals and spirals is designated as lenticulars (S0's). Galaxies on the left of the diagram are called ‘early’ and on the right ‘late’ in type [9].

His study was based on imaging technique, i.e., galaxy photographs, which is one of the effective ways of studying galaxy evolution. According to Hubble some galaxies are challenging to understand in the context of the tuning fork diagram. These consist of dwarf galaxies, which are very small, giant elliptical galaxies, which are extremely huge elliptical galaxies seen in the centers of some clusters of galaxies, and irregular galaxies, which

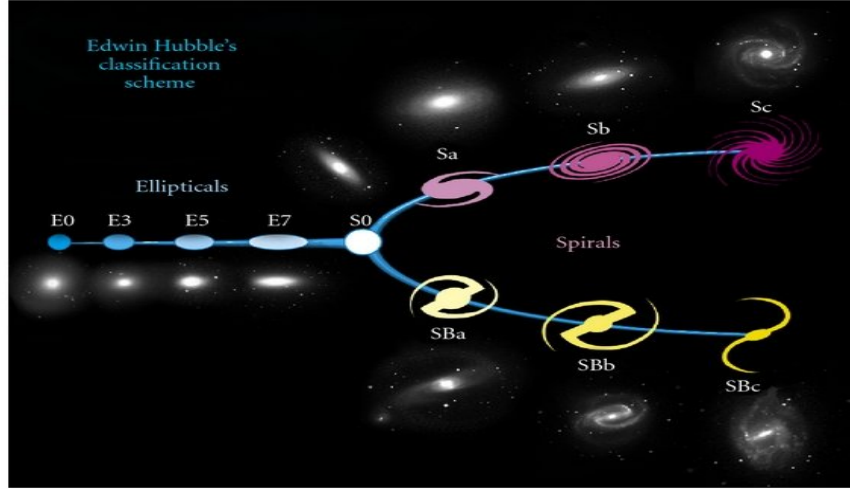


Figure 1: The Hubble tuning fork diagram. A schematic view of the Hubble galaxy classification. Credit: NASA and ESA.

have strange shapes. Recent studies suggest that galaxies are in different shapes and morphology due to evolutionary processes. These evolutionary processes are driven by physical properties, such as galaxy mass, angular momentum, and gas in-flow and out-flow. The sections below describe some of the important type of galaxies.

2.1.1 Spiral galaxy



Figure 2: Credit: M51: NASA/JPL-Caltech/Univ. of Arizona/DSS/SST; CenA: NASA/DOE/Fermi LAT Collaboration, Capella Observatory.

Spiral galaxy are not only visually appealing but, they also tell us important information about star-formation. Spiral galaxies are known to be

star-forming, which is an important scenario to study the astrophysics of galaxies, chemical enrichment and hence the galaxy evolution.

The fun facts are: when hydrogen gas falls in dark matter halo, it star rotation to balance the angular momentum of dark matter halo and it own. Subsequently, gas falls towards the centre, maintaining its rotation (in some cases also referred by angular momentum), and cools down. Gradually, gas clouds starts fragmented due to gravitational instabilities. These fragmented gas clouds hosts the star-formation. In general spiral galaxies disc like system and their spiral arms host most of the star forming activities.

2.1.2 Elliptical galaxies:

Elliptical are named after their shape which is spheroidal shape and stars wrap around the center of the galaxy in all directions equally. As mentioned in Section 2.1.1, when a galaxy run out of the gas reservoir and star-formation stops. At this stage a galaxy is generally concentrated with stars (relatively old stars). New star-formation doesn't take place in elliptical galaxies. In these galaxies stellar pressure dominates while in spirals gas pressure. This why study of elliptical galaxies is mostly done using stellar motion (i.e. stellar continuum). They are the massive i.e: high mass galaxies. Elliptical galaxies vary in terms of their sizes and masses, which it ranges between 10^5 to nearly 10^{13} solar masses. Consider the galaxy shown in figure 3

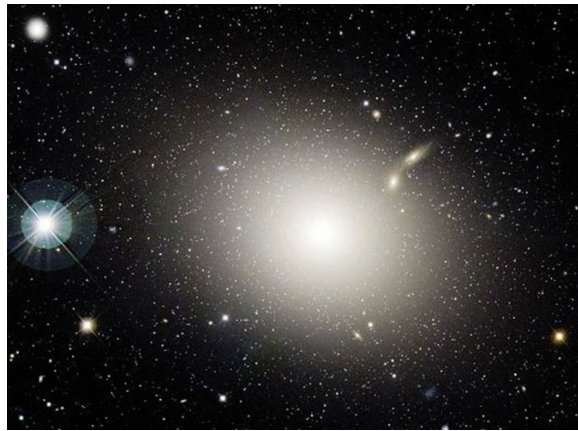


Figure 3: Hubble classified **M87** an elliptical extra-galactic nebula with no apparent elongation (class E0), as a member of the Virgo Cluster and estimated its distance from Earth to be 1.8 million parsecs (5.9 million light-years). Credit: Canada-France-Hawaii Telescope,

2.1.3 Irregular galaxies

These galaxies are formed when spiral galaxies collide [3] while the still have gases in them. That gas get compressed and collapses into new stars. Then they can be classified as star burst galaxies. They contain bright blue stars(young stars) that are just formed from the merging process. These galaxies have no symmetrical shape, some are young hot stars, others have obscured stars and they are not as large as spiral or elliptical galaxies. When using the tuning fork 1, the irregular galaxies are at far right of the fork and their classification cannot be defined. These include the small and large Magellanic cloud which are quite a bit smaller galaxies. The LMC has a prominent bar in the center and was most likely a barred spiral galaxy before colliding with the Milky Way. The LMC is about ten times smaller in size and between ten and one hundred times smaller in mass than the Milky Way. It has a lot of gas and a lot of active star formation areas. The LMC contains some of the most well-known star-forming regions.



(a) NGC 55 irregular galaxy. Credit: Don Goldman



(b) The famous Large Magellanic Cloud (LMC). Image Credit: Primoz Cigler

Figure 4

2.1.4 Dwarf galaxies

We have types of dwarf galaxies i.e dwarf spheroidal, ultra-faint dwarf[7], dwarf elliptical and ultra-compact dwarf galaxies. Dwarf irregular galaxies have an ongoing star formation while the dwarf elliptical does not. Dwarf galaxies are dark matter dominant (as they have less stars and gas) which makes them ideal systems to test dark matter(DM) models. These galaxies' star-formation and chemical enrichment histories are complicated, diverse, and frequently initiated by and perpetuated by as-yet unidentified mechanisms. An example being UGC 4459 [6], they are very abundant and have wide variety of shapes. We also have the Fornax Dwarf Spheroidal an elliptical dwarf galaxy in the constellation Fornax. The dwarf galaxies are the most prevalent type of galaxy across the Cosmos is the dwarf galaxy. They greatly add to the universe's mass, but because they are small and poorly

illuminated, very little is known about them.

2.2 Various Galaxy Components

The disk of galaxies contain a substantial fraction of their baryonic matter. The evolutionary activity in these galaxies, such as the formation of stars, spiral arms, bars and rings and the various forms of secular evolution takes place in their disks. Every galaxy form and evolves in a dark matter halo, and so the disk galaxies. Therefore, in order to understand the nature of dark matter in galaxies, it is essential to study the various components of disk galaxies such as, stellar disk, gas disk, globular clusters, stellar bulge, etc. In this section we give a brief summary on various components of disk galaxies.

2.2.1 Dark Matter Halo

A halo is a galaxy's extended, roughly spherical component that extends beyond the visible component. The stellar halo is a population of stars and globular clusters that is thought to surround most disk galaxies and the elliptical galaxies of type-CD. A dark matter halo is a fundamental building block of cosmological structure. It is a hypothetical region containing gravitational bound matter that has decoupled primordial matter during cosmic expansion (Dark matter halo). The inferred halo of invisible material (dark matter) that permeates and surrounds individual galaxies, as well as groups and clusters of galaxies, is referred to as a dark halo. Hypothetically, the formation of dark matter halos is thought to have played a significant role in the formation of galaxies.

2.2.2 Globular cluster

The globular cluster is an extremely dense stellar cluster. These are stable tightly bound clusters of tens of thousands to millions of stars. Globular Clusters are associations of stars with a typical size of a few pc to 10 pc. They are associated with all types of galaxies. Globular clusters are typically much larger than open clusters and are tightly gravitationally bound. Globular Clusters are much older than open clusters and have typical ages close to the age of the universe. Since they are very dense, they therefore display a rich dynamical phenomenology that is quite different from its galaxy. They can be disrupted by tidal interactions with their host galaxy, leading to the production of narrow stellar streams (a stellar stream is an association of stars orbiting a galaxy that was once a globular cluster or dwarf galaxy that has now been torn apart and stretched out along its orbits by tidal forces). Consider the figure 5,

The Milky Way has about 150 globular clusters, the number of globular clusters in a galaxy scales with the total mass. M80 is one of the most



Figure 5: Image of NGC 5907 stellar streams

massive of the 150 globular clusters in the Milky Way.

2.2.3 Stellar disk

The stellar disk is the flat part of a spiral galaxy around the central bulge. The disk can be thought of as being the underlying body of stars upon which arms are superimposed. This body has a thickness that is roughly one fifth of its own diameter, but different components have different characteristic thickness. The thinnest component often called the "Thin Disk" composed mostly of stars, and very little gas which is unaccountable. The thin disk contains stars with a wide range of ages and may be divided into a series of sub-populations of increasing age. Whereas, the thickest component, the "Thick Disk" composed of older stars. Spiral galaxies have more prominent stellar disk.

2.2.4 Gas Disk



Figure 6: Stellar and gas disk of m87

Disk galaxies have both a thin and thick disk component. A thick disk

forms in early period of galaxy and grows with time, becomes thicker, and enriches in metal and stars . Whereas thin disk takes place in later time, star-formation is relatively new in it. However most of the interstellar gas is contained within the galaxy's thin disk and it constitutes approximately 10% of the total baryonic mass. The gas itself is difficult to observe, but its composition and distribution can be traced by interstellar dust. Our Milky-way also have thin and thick gaseous disk.

2.2.5 Stellar Bulge

The term ‘bulge’ is used to describe the dense spheroidal swarm of stars often found in the centres of spiral and S0 galaxies [1]. The bulge of the Milky Way appears to be fairly typical – a slightly flattened sphere of radius $\approx 6,500$ light years – while bulge sizes in other galaxies vary from several hundred to several tens of thousands of light years, depending on the type and size of the galaxy. Within the bulge, stars orbit in a completely random fashion meaning that the bulge is velocity dispersion supported rather than rotation supported.

The ages of bulge stars is a topic currently under investigation. Until recently, stars in the bulge our own Galaxy were all thought to be old, population II stars.

2.2.6 Black hole

Black holes are the most extreme objects in the universe. Supermassive versions of these unimaginably dense objects likely reside at the centers of all large galaxies. Stellar-mass black holes—which weigh approximately five to 100 times the mass of the sun—are much more common, with an estimated 100 million in the Milky Way alone. A black hole is a region of space-time where gravity is so strong that nothing – no particles or even electromagnetic radiation such as light – can escape from it.

Black holes of stellar mass form when massive stars collapse at the end of their life cycle. After a black hole has formed, it can grow by absorbing mass from its surroundings. Supermassive black holes of millions of solar masses (M_{\odot}) may form by absorbing other stars and merging with other black holes

The presence of a black hole can be inferred through its interaction with other matter and with electromagnetic radiation such as visible light. Any matter that falls onto a black hole can form an external accretion disk heated by friction, forming quasars, some of the brightest objects in the universe. Stars passing too close to a supermassive black hole can be shredded into streamers that shine very brightly before being ”swallowed.” [4] If other stars are orbiting a black hole, their orbits can determine the black hole’s mass and location. Such observations can be used to exclude possible alternatives such as neutron stars. In this way, astronomers have identified numerous

stellar black hole candidates in binary systems and established that the radio source known as Sagittarius A*, at the core of the Milky Way galaxy, contains a supermassive black hole of about 4.3 million solar masses.

2.3 Summary

In chapter 2, we have discussed the types of galaxies and galaxy components. This lays the path for our aim as we look into galaxy dynamics and their dark matter content. Understanding the various components of galaxies will help us in understanding the kinematics of the galaxy and how we can classify them for each component. To further understand the kinematics, we will look into the dynamics where we model the motion of these components. Therefore, in the sections below we look into Galaxy kinematics, Dynamics and present the results of our project.

3 Galaxy Kinematics

3.1 Observations

Galaxy kinematics is a way to measure the motion of stars and gas that allows us to obtain fundamental information about the formation of galaxies and their current dynamical state. In this section I present the techniques of obtaining galaxy kinematics.

3.1.1 Conventional Spectroscopy

A conventional method of determining the motion of stars and gas in a galaxy is slit spectroscopy. Depending on the scientific goal, one can use a long narrow slit or a wide slit. For studying extended objects (such as galaxies), a long narrow slit is recommended [8].

The light rays coming from an object as they pass through the slit are exposed to the spectrograph, which produces the spectrum along the horizontal axis of the slit, where the vertical axis of the slit gives the spatial information. The spectrum of a galaxy generally contains absorption, emission and the continuum. These, absorption and emission features in the spectrum of galaxy (or any object) are the key to unlock its composition, element abundance, temperature, pressure and motion plus distribution of stars and gas. To derive the galaxy kinematics, we generally study the Doppler-shift in the peak (or dip) of the emission (or absorption) lines. See Box 3.1.1.

Box 1

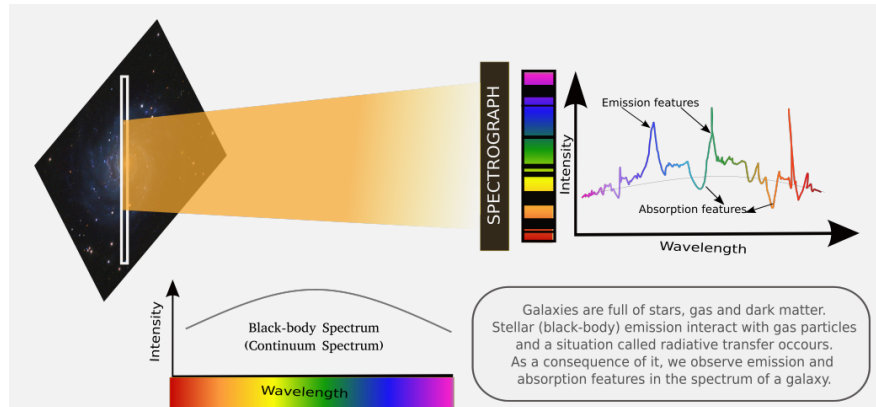


Illustration of a conventional method of recording the spectrum of galaxies and its properties. In principle, the light rays coming from the stars in the galaxies should form a continuum spectrum (black-body), but because of the presence of gas particles, some of the light is absorbed and a part of it radiates even with higher intensity. The former corresponds to absorption and the latter is called an emission feature. For example, a continuum feature can be represented by a rainbow slab, where dark lines on this rainbow slab represent absorption and bright lines represent emission. Astronomers study these features to determine the kinematics and dynamics of a galaxy (or galaxies, also stars and gas)[8].

The Doppler-shift ¹ connects the Line of Sight Velocity (V_{Los}) ² of the object with its emitted wavelength (or frequency):

$$\frac{V_{Los}}{c} = \frac{\lambda_{obs} - \lambda_{emit}}{\lambda_{emit}} = \frac{f_{obs} - f_{emit}}{f_{emit}} \quad (1)$$

where, λ_{obs} and λ_{emit} are the observed and emitted (at rest frame of the source) wavelengths, respectively. The cosmological red-shift (z) of the object is given by $z = \frac{V_{Los}}{c}$, where c is the speed of light. At this stage it is imperative to pinpoint that the galaxy as a whole is moving away from us due to the expansion of the universe, this motion is called the recession velocity

¹When a body that is emitting radiation has a non-zero radial velocity relative to an observer, the wavelength of the emission will be shortened or lengthened, depending upon whether the body is moving towards or away from an observer. This change in observed wavelength, or frequency, is known as the Doppler shift.

²**Line of Sight Velocity (V_{Los})** is the radial velocity also known as radial speed or the range rate of a target with respect to an observer that is the rate of change of distance or the range between the two points (target and observer). This rather denotes the speed with which the object moves away from the earth or observer (red-shift) or approaches it for a negative radial velocity (blue-shift)

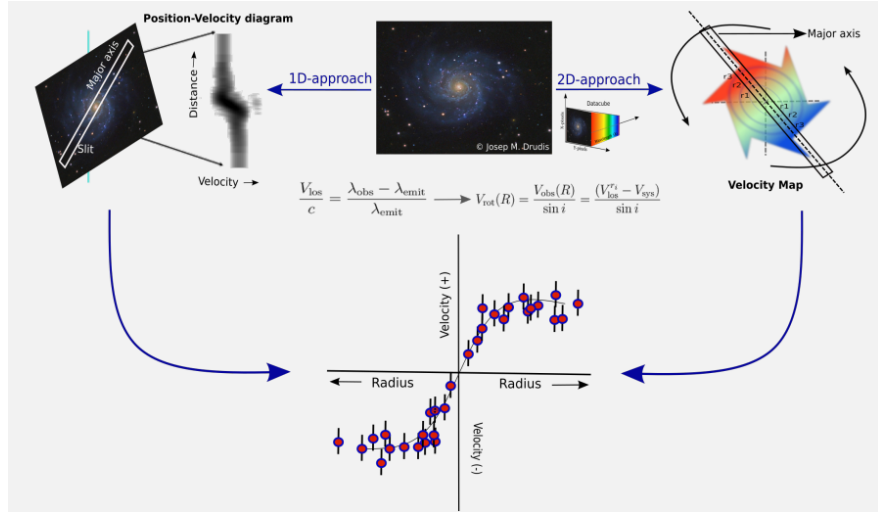
(V_{res}) of the galaxy. The galaxy has local motion due to local gravitational effects, so-called peculiar velocity (V_{pec}). Then the sum of the peculiar velocity and recession velocity of a galaxy gives Systematic Velocity ³ i.e, $V_{sys}=V_{res}+V_{pec}$, which is measured in sun's rest frame, that is by accounting the heliocentric velocity ⁴. In addition to V_{sys} , the gas and stars of the galaxy rotate around the centre of the galaxy at a certain speed, called the rotational velocity V_{rot} . In principle, the line-of-sight velocity inferred from the Doppler effect is the sum of $V_{rot} + V_{sys}$, i.e., to determine the true observed rotation velocity, we need to separate these two velocities. In general, an average velocity of stars within the galaxy or velocity about its centre of mass equals to the systemic velocity. Providing this information, the observed rotation velocity of the galaxy is $V_{obs} = V_{rot} + V_{sys}$.

An example of rotation curve derived from slit-spectroscopy is shown in Box 3.1.1. Deriving the rotation curves from slit spectroscopy is quite simple and fast, but it has several drawbacks: 1) the spatial information perpendicular to the slit is indeterminate; 2) light outside the slit is always lost; 3) to study the kinematics in the whole galaxy, we need to repeat the observation several times, which is time-consuming and expensive; 4) to obtain the rotation curve, the slit is generally placed along the major axis, since this gives us the averaged rotational velocity of a galaxy. However, if the angular size of the object is small, especially for high-redshift objects, then it is difficult to guess the axis information; 5) the triaxial component of the velocity field and the line strength distribution of a galaxy provide rich information about its present dynamical state, which is difficult to measure with slit spectroscopy. We introduce Integral Field Spectroscopy, a technique which surpasses the limits and difficulties of Conventional Spectroscopy.

³**Systematic Velocity** V_{sys} is the average velocity of the galaxy, or the velocity of its center of mass. It is important because when the galaxy rotates the different phases move differently, where we have stars on one side with different velocities than those stars on the other side.

⁴The Heliocentric velocity is the velocity defined with respect to a frame in which the Sun is at rest

Box 2



One- and two-dimensional approaches to deriving rotation curves. In the onedimensional (1D) approach, we place the slit along the major axis of the galaxy and obtain the spectrum using the step-up shown in Box 3.1.1. In the two-dimensional (2D) approach, we first obtain the spectrum using integral field spectrographs, as shown in Figure 7, which comes in the form of a datacube. This datacube is then reduced to the velocity map (the velocity map can also be derived using slit spectroscopy, but this process is time consuming). In both the 1D and 2D approaches, the Doppler effect is used as the basis for deriving the observed velocity. As can be seen from the figure, the main difference between the two studies is that in the 1D-approach the velocity is observed along the major axis of a galaxy, while in the 2D-approach the velocity is observed over the entire galaxy, which is then averaged along the major axis, resulting in the rotation curve similar to the 1D approach. Finally, we can note that the rotation curve has two arms, one indicating the positive velocity and the other the negative velocity, representing respectively the receding and approaching parts of the galaxy with respect to the observer's rest frame [8].

3.1.2 Integral Field Spectroscopy

Integral Field Spectrograph (IFS) came with the goal of studying triaxial motion, resolved kinematics, and extended objects (e.g., galaxies). IFS uses the Integral Field Units (IFUs), which collects light from each pixel and transmits it to the spectrograph without any loss. Many advanced IFUs have been developed since the 2000s, and they can be designed in many different ways. Refer to figure 7 for the three commonly used IFU+IFS designs,

where, (1) Lenslets uses micro lens arrays that split the image into small light sources, then each light source is placed in the spectrograph entrance (same slit plane) and exposed to the disperser, resulting in a spectrum. The system is tilted to avoid the overlap of each lenslet spectrum. (2) Lenslets plus fibers IFU is very similar to lenslet IFU, but in this case each lenslet focuses the light beam on the optical fiber and behaves like a pseudo-slit, which is then transmitted to the disperser to produce the spectrum.(3) Image Slicer: As the name suggests, the image is sliced and then each slice is reformatted into a pseudo-slide, then the light is exposed to the disperser to obtain the spectrum. An image slicer uses mirrors to form and reform the image.

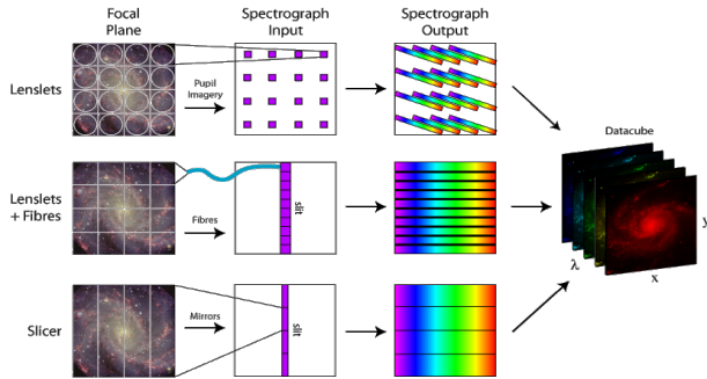


Figure 2.1: Types of Integral Field Units, image credit [Westmoquette \(2007\)](#).

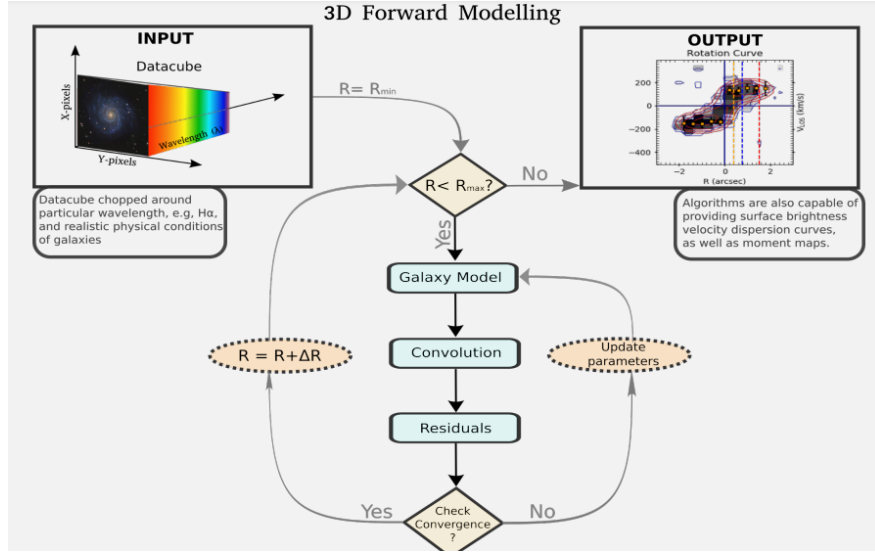
Figure 7: : Types of Integral Field Units

The spectrum of an IFU is always rearranged in the $x - y$ position of the galaxy as a function of wavelength, creating a $datacube = f(x, y, \lambda)$ that gives the 2D observations a three-dimensional appearance[8]. The datacube is used to derive the rotation curves.

Recently, scientific community have made progress in developing 3D algorithms for inferring rotation curves (and other properties) from datacubes, for example GALPAK-3D, and BLOBBY-3D. These algorithms are capable of directly fitting the flux of datacube, generating mock datacube, and comparing the data and models using robust statistics that take into account the instrumental response (line and point spread function). As a result, they proved to be relatively robust in determining the accurate rotation curves. A schematic diagram of the 3D approach to derive the rotation curves is shown in Box 3.1.2.

Furthermore, we use either stellar or gas kinematics to derive the rotation curves. With current instrument capabilities, both stellar and gas kinematics are accurately measured for local galaxies.

Box 3



Schematic representation of the 3D forward modeling algorithm. In 3D forward modelling, we input the entire data along with some initial guesses about the physical conditions of the galaxy. In particular, we provide 1) three geometrical parameters of galaxy: position inclination angle, central x y coordinates, which are estimated from photometry; 2) guess on kinematic parameters rotation velocity and velocity dispersion; 3) instrument response: Point Spread Function (PSF) and the Line Spread Function (LSF); and 4) depending on the distance of galaxy, one also needs to provide redshift information. For a given geometrical and kinematical parameters, the algorithm generates a mock datacube. This mock datacube is then convolved for the instrumental response. Then, the flux in the observed and mock datacubes is compared using some statistics (e.g., Bayesian), which allows to modify the initial guesses until the convergence occurs. In the end, the observed rotational velocity, velocity dispersion, and surface brightness is calculated ring by ring. Note, here the algorithm used in 3D-BAROLO is described. However, with different software/algorithm, technical details (e.g., galaxy model) may differ, but the general structure and idea remains the same.

I have worked on the data of NGC2403, see section 3.2

3.2 Data

In this section I present data on the chosen galaxy with reference to [2] and clarify the tools I used to perform the analysis to achieve our goal.

Component	Value
Name	NGC2403
Stellar Mass (MD)	$3 \times 10^{10} M_{\odot}$
HI Gas Mass (MHI)	$10^9 M_{\odot}$
Effective Radius (RE)	$7.6 kpc$
Stellar Radius (RD)	$0.59 \times RE(kpc)$
HI gas radius (RHI)	$3 \times RD$
Central X-Position	77
Central Y-Position	77
Systematic Velocity	$132.8 km/s$
Observations	HI 21cm
Pointing R.A. (J2000)	07 36 54.5
Pointing Dec (J2000)	+65 35 20.0

I derived the kinematics of NGC2403 using 3D Barolo, see section 3.3.

3.3 Barolo

3D-BAROLO (3D-Based Analysis of Rotating Object via Line Observations) is a 3D fitting tool for the kinematics of galaxies[2]. Here, line observations mean, we only study the emission lines, which is beneficial for radio observation (21 cm emission, i.e., neutral hydrogen), as well as for high and low red-shift Universe.



Figure 8: Barolo logo

3D BAROLO (hereafter 3D Barolo or Barolo) is based on the 'titled ring model' i.e., the motion of the gas and stars are assumed to be in the circular orbits. It does not assume any functional evolution of kinematic quantities (e.g., $V_{rot} \propto \tan^{-1}(R)$)

To understand how Barolo works, consider the diagram below

Barolo require observed datacube, kinematic parameters (V_{rot} , V_{dip} , redshift), and geometric parameters (galaxy centers, inclination and position angle). Based on this it creates a modelled datacube, this data cube is convolved for instrumental information (i.e., point spread function, line spread function). The convolved modeled cube is compared with observed datacube using state-of-art minimization techniques (MCMC sampling). This process yields best fit datacube, moment maps, position velocity diagrams, and radial profiles (of velocity dispersion and intensity). All this information is detailed in sections below.

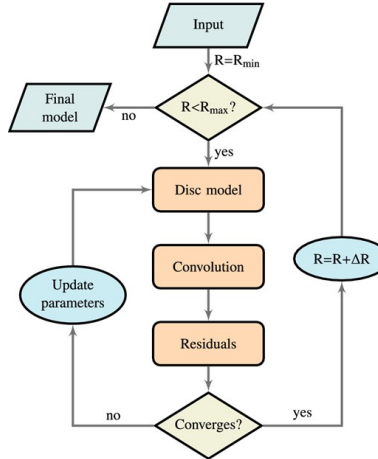


Figure 9: Flowchart of the 3D BAROLO main algorithm. For each ring R , the algorithm builds a 3D model, convolves it with the observational beam/PSF and compares it with the data. If no convergence has been achieved, 3D BAROLO updates the parameters and starts over. When the algorithm converges to the minimum, it moves to the next ring. The optional normalization step takes place after the convolution step.

3.3.1 3D Barolo installation

I learned installing Barolo on Linus and Windows operating systems.

3.3.1.1 Requirements

Normally when you introduce a new language into a system, you have to prepare an environment to ensure that your program runs smoothly, so it follows that the same is true for installing BBarolo, note that this software/tool is developed using C++ hence the following are required to successfully compile Barolo:

- C++ environment
- CFITSIO library
- FFTW library
- WCS library
- QT toolkit
- Gnuplot and Python

3.3.1.2 Compiling

Given that your system satisfies all requirements you'll successfully install 3D-BBarolo however if like my system which did not have all the requirements, there will be problems along the way. following the instructions here

I successfully downloaded, uncompressed the files however, I couldn't configure successfully because I had the WCS library missing. To fix this I went to the home site of WCS to try and find out as to how should I install this library. The individual attempts resulted into a lot of learning and failure, however, I approached some experts in computation and I successfully got help. I had to download, decompress, configure, make and make install the wcs library. Finally I tried to configure Barolo which ran successfully. Thereafter, I compiled, make and make install as per instructions. After these steps I successfully installed Barolo. To check that, I went to the terminal and typed: \$BBarolo, and the terminal fills with Barolo tag, as shown in Figure 10



The image shows a terminal window with a black background and white text. At the top, it displays the command: `nhlakaniph@LAPTOP-J1MRBS80:~$ BBarolo`. Below this, there is a decorative graphic composed of various ASCII characters like parentheses, brackets, and dots, forming abstract shapes. In the center of this graphic, the text "BBarolo quick guide" is written. To the right of the graphic, there is another decorative element consisting of brackets and the word "BAROLO" followed by the year "2015".

Figure 10: Output of successful installation of 3d-Barolo

3.3.2 Barolo Inputs

BBarolo takes input parameters specified through a parameter file. A parameter file is a text file that contains a list of parameter names and values. This parameter file is saved with extension '.par', for example, galaxy_name.par. This is the input file, parameter names are not case sensitive and lines can be commented out using # or //. The order in which parameters are listed has no effect on running the Barolo. However, if a parameter is listed more than once then only the last value is considered as the latter overwrites the former. We have mandatory and optional parameters. Parameters which have not been specified set to default values. See an example of par file in Figure 11.

```

n2403 - Notepad
File Edit Format View Help
FITSFILE    ngc2403.fits
THREADS      4
3DFIT        true
NRADII       41
RADSEP       30
VSYS         132.8
XPOS         77
YPOS         77
VROT         120
VDISP         8
INC          60
PA           143.7
Z0           10
FREE         VROT VDISP PA
LTYPE         2
FTYPE         2
DISTANCE     3.2
MASK         SEARCH
WFUNC         2
TWOSTAGE     true
FLAGERRORS   true

```

Figure 11: Parameter file

3.3.2.1 General Parameters

- **FITSFILE:** this is a mandatory parameter, for all fitting tasks, it contains the name of the input FITS file.
- **THREADS:** this gives us the number of CPUs to use for task execution.
- **3DFIT:** this enables 3D fitting algorithm. Can be set to true or false
- **NRADII:** gives the number of rings to be used and fitted.
- **RADSEP:** separation between the rings in arcsec
- **VSYS:** systematic velocity in km/s.

- **XPOS:** X-center (x center coordinate) of galaxy
- **YPOS:** Y-center (y center coordinate) of galaxy
- **VROT:** rotation velocity in km/s
- **VDISP:** velocity dispersion in km/s
- **INC:** inclination angle in degrees
- **PA:** position angle in degrees of the receding side of the galaxy
- **Z0:** scale-height of the disc in arcsec

3.3.2.2 Main Options

We have main options, which are important parameters that can be used to control 3DFIT.

- **FREE [VROT VDISP INC PA]** this parameter contains a list of parameters to be fitted.
- **MASK** tells the code how to build a mask to identify the regions of a genuine galaxy emission. Set to SEARCH which specifies the source finding is ran and the largest detection used to determine the mask.
- **TWOSTAGE** set to true, this flag enables the second fitting parameter regularization. This is relevant if the user wishes to fit other parameters other than VROT, VDISP and VRAD.
- **FLAGERRORS** set to true, code will estimate the errors hence slowing down the run.

3.3.2.3 Advanced Options

We have the advanced options which are additional optional parameters to refine the fit.

- **LTYPE** a function used to fit the intensity along the z axis
- **FTYPE** function to be minimized.
- **WFUNC** weighting function to be used in the fit. Value = 2 for $\cos^2 \theta$ and θ is the azimuthal angle.

3.3.2.4 Beam Parameters

The following parameters are used to specify the size and shape of the Point Spread Function (PSF or beam). These parameters are ignored if beam information is written in the header of the input FITS file, either through BMAJ, BMIN and BPA keywords or in the HISTORY. The code defines the beam following the priority order: header → bmaj,bmin,bpa params → beamfwhm param → default to 30 arcsec.

- **BMAJ** gives the FWHM of the major axis of the elliptical Gaussian beam in arcsec.
- **BMIN** gives the FWHM of the minor axis of the elliptical Gaussian beam in arcsec.
- **BPA** gives the position angle of the major axis of the elliptical Gaussian beam in degrees, counter-clock from the North direction.
- **BEAMFWHM** gives the FWHM of a circular Gaussian beam in arcsec.

3.3.3 Barolo Outputs

3.3.3.1 Channel Maps

Channel Maps These contain a channel-by-channel comparison of data and models, shown in Figure 12. In blue, the top panel we have the data or

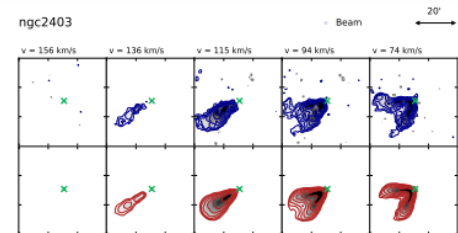


Figure 12: Channel maps

observed data and in the red bottom panel we have the model. Each block is a map at different frequency (velocity) channels. The map corresponding to the systematic velocity of the galaxy is shown in the centre. Despite the observations having an uneven noise distribution, Barolo is able to reproduce the data very well and in particular it traces the prominent warp visible as a deformation of the channel maps in the outer regions of the galaxy.

3.3.3.2 PV Diagram

PV Diagram contain a position vs velocity comparison of data and model taken along the average major and minor axis an example is shown in Figure 13. Where the black shaded area with the blue contours represents the data,

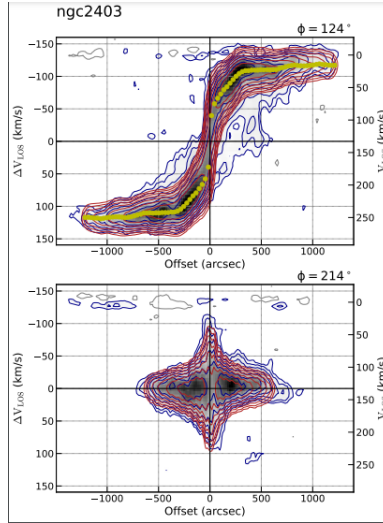


Figure 13: PV Diagram

the red contour is the model and the yellow squares with the yellow squares with error bars are the best fit measurement of the Line of sight velocity (V_{los}). This diagram is usually called the rotation curve which is a plot of the rotational velocity of gas in a galaxy versus their radial distance from the galaxy's center.

3.3.3.3 Moment Maps

Moment Maps contain a comparison of data and model moment maps. Moments are a way to reduce the size of a large data set into few key numbers (e.g. mean, standard deviation). A moment map is when you repeat that process for every pixel of an image (creating a "map"), an example is shown in figure 14.

There are 3 moment maps:

- M0 - Intensity (Surface brightness)

$$\int I_v dv \quad (2)$$

- M1 - Rotational Velocity

$$\int (v) I_v dv \quad (3)$$

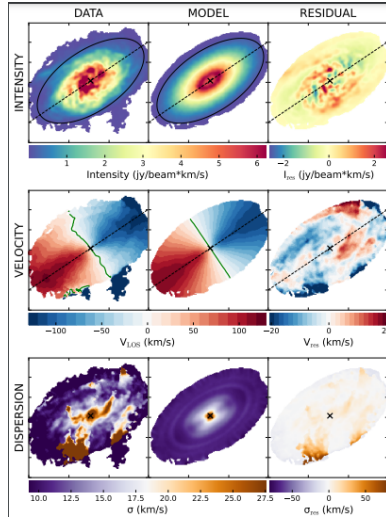


Figure 14: Moment maps

- M2 - Velocity Dispersion

$$\int (v^2) I_v dv \quad (4)$$

In figure 14, the black-grey dashed line shows the position angle, and the black across shows the galactic center. We have 3 by 3 maps, data moments maps, modelled moments maps and the residual maps. In the Intensity Map, we have high intensity at the center and low intensity as we move away from the center, which confirms the exponential intensity profile. The Velocity map, we can see the red and blue colours which refer to the red-shift and blue-shift velocities respectively. Dark blue velocities relating to high velocities at which a galaxy is coming towards us as observers and dark red referring to high velocities of a galaxy moving away from us. The Dispersion Map then shows the mean velocity for a group of objects with the blue area being a location of low velocities to and the brown/orange depicting high velocity dispersion's. Notice that at the center velocity dispersion is higher than the edges of galaxies, it is due to the radiation pressure from stars, which introduce random motion in system.

3.3.3.4 Ring files

Rings file contains the best fit parameters namely (VROT, VDISP AND PA). See an example in figure-15.

In figure 15 graphs contained in the rings file, are the plots of best fit parameters. In the first row, we have the plots of velocities as a function of

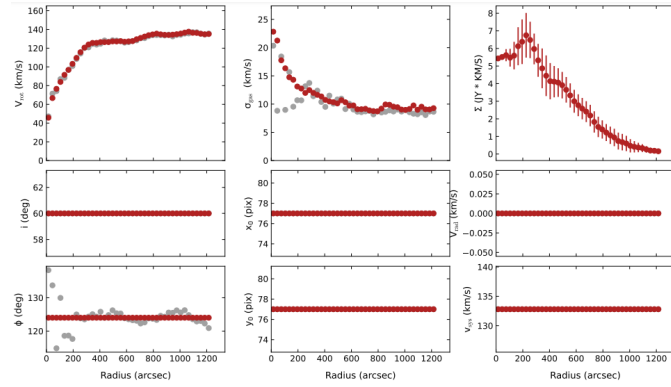


Figure 15: Best Fit Parameters

radius in arcseconds. We have V_{los} and V_{disp} . In the second row we have the plots of Inclination angle, Central X position and Radial velocity as a function of radius. In the third row we have the plots of Position angle, Y central position and Systematic velocity as a function of radius. Notice that in 2nd and 3rd row, all our values are constant throughout the change in radius which suggest that these do not change as radius changes, they are fixed parameters. However, those in first row are affected by the change in radius as they either increase or decrease due to radius. We can see that the plot of V_{los} is a rotational curve of the observed velocity of the galaxy.

4 Galaxy Dynamics

4.1 Stellar Disk

The Stellar disk has light profiles that follow exponential functions in both the radial and vertical directions.

1. Radial Profile: The surface brightness radial profile of the galactic disk roughly follows an exponential function.

$$I(R) = I_o \exp\left[-\frac{R}{h_R}\right] \quad (5)$$

where, I_o is the galaxies central brightness, h_R is the scale length. The scale length is the radius at which the galaxy is a factor of $e(2, 7)$ less bright than it is at its center, also known as disk radius R.D. Due to the diversity in the shapes and sizes of galaxies, not all galactic disks follow this exponential form in their brightness profiles. Some galaxies have been found to have discs with light profiles that have been shortened as time goes by.

2. Vertical Profile: The vertical surface brightness profiles of galactic disks follow an exponential profile that is proportional to the discs radial profile:

$$\begin{aligned} I(R, Z) &= I(R) \exp\left[-\frac{|z|}{h_z}\right] \\ &= I_o \exp\left[-\left(\frac{R}{h_R} + \frac{|z|}{h_z}\right)\right], \end{aligned} \quad (6)$$

where, $h_z \approx 0.1h_R$ is the scale height. Although exponential profiles serve as a useful first approximation, vertical surface brightness profiles can get complicated, for example a case where the scale height h_z increasing with the radius. We assume that the distribution of stars in local and high-redshift star-forming galaxies are in exponential discs, so that the surface densities can be written as (up to a geometric factor) [8]:

$$\Sigma(R) \propto \frac{M}{R_{scale}} \exp\left(-\frac{R}{R_{scale}}\right) \quad (7)$$

where, M_i and R_{scale} are the total mass and the scale length of the different components(stars, H2, HI), respectively. Note that stellar mass in the disc (without bulge) is denoted by MD, while the contribution of the total stellar mass is represented by (M_\odot or $M_{star} = MD + M_{bulge}$). Assuming the above density distribution of the stars, their contribution to the circular velocity of the disc can be expressed as follows:

$$V_{stellar}^2(R) = \frac{1}{2} \left(\frac{GM}{R_{scale}}\right)(x^2)[I_0K_0 - I_1K_1], \quad (8)$$

where, $x = \frac{R}{R_{scale}}$ and I_n and K_n are modified Bessel functions computed at $1.6x$ for stars.

4.2 Gas disk

The interstellar gas can be separated into five different phases, namely very cold star-forming molecular gas clouds (mostly H_2), cold atomic gas clouds (mostly neutral atomic hydrogen HI), warm neutral gas surrounding the cold clouds, hot ionised gas regions around hot stars (mostly ionised hydrogen HII), and very hot, diffuse and ionised coronal gas.

The molecular hydrogen (H_2) content can be traced by carbon monoxide molecules and is generally confined most closely to the midplane of the galaxy with relatively small vertical scale heights, and radially close to the galactic centre. Atomic neutral hydrogen HI extends radially outwards to the edge of the galactic disk and in the outer regions of the galaxy the vertical scale height of HI increases exponentially and is much less confined to the galactic plane, flaring out at the edges and often exhibiting a warp-like distribution. (warped image)

The gas in the disk is not uniformly distributed in either radial or vertical directions, there are bubbles of hot diffuse gas mixed with clumps and clouds of cooler, more dense gas. The various gas components tend to move in approximately circular orbits around the centre of their disk galaxies, with velocities proportional to the luminosity of the galaxy. However, observations report that for local disk galaxy gaseous disk component is uniform, i.e., follows a similar light distribution as stellar disk. Given this, the velocity profiles of gaseous disk is defined as:

$$\sum(R) \propto \frac{M}{R_{scale}} \exp\left(\frac{-R}{R_{scale}}\right) \quad (9)$$

where, M_i and R_{scale} are the total mass and the scale length of the different components(stars, H_2 , HI), respectively. Note that stellar mass in the disc (without bulge) is denoted by MD, while the contribution of the total stellar mass is represented by (M_\odot or $M_{star} = MD + M_{bulge}$). Assuming the above density distribution of the stars, their contribution to the circular velocity of the disc can be expressed as follows [8]:

$$V_{gas}^2(R) = \frac{1}{2} \left(\frac{GM}{R_{scale}} \right) (x^2) [I_0 K_0 - I_1 K_1], \quad (10)$$

where, $x = \frac{R}{R_{scale}}$ and I_n and K_n are modified Bessel functions computed at $0.53x$ for gas.

4.3 Stellar bulge

The stellar bulge is a structure independent to the disks of disk galaxies and is composed of groups of stars found in the central regions of the galaxy.

The surface brightness of stellar bulges can be described as a Sersic profile:

$$\mu(R) = \mu_0 - b_n R^{1/n} \quad (2.4.1)$$

Where $\mu(R)$ describes the surface brightness as a function of radius, μ_0 denotes the central surface brightness, n is known as the Sérsic index, and b_n is computed from n . The bulge dominates the mass and luminosity

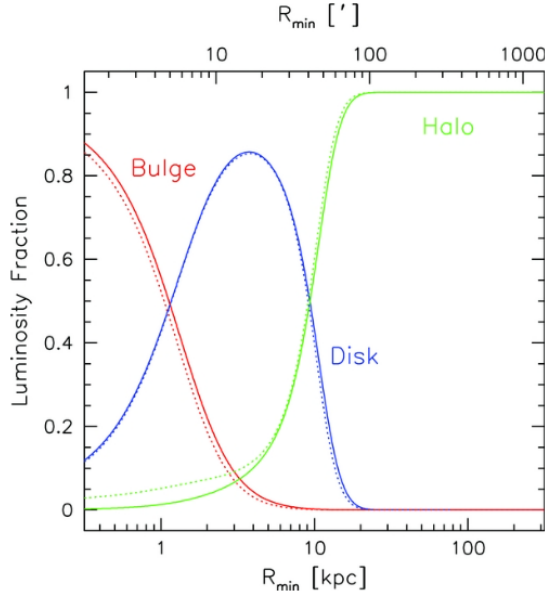


Figure 16: The luminosity contributions of M31’s bulge, disk, and stellar halo as a function of radius. The dashed red line is M31’s bulge component and the solid red line is the Sérsic bulge profile, the bulge dominates within 1kpc.

contribution in the central region of the galaxy. Classically spheroidal bulges tend to be home to mostly older, Population II stars, and are hence reddish in colour. The spheroidal shape is due to the stars in these types of bulges orbiting the centre somewhat randomly relative to those in the disk, which is thought to be the result of collisions or mergers. Generally there is very little star formation occurring in the bulge, since there is insufficient dust and gas. Look Figure 16 for xyz.

The chemical abundances and metallicities of the stars in the stellar bulges varies quite significantly, in the Milky Way there are three distinct age groups: (i) very young (< 200 Myr) (ii) Medium (200 Myr up-to 7 Gyr) and (iii) Very old (> 7 Gyr, up to ~ 10 Gyr). Interestingly, the oldest population of stars also have the highest metallicities, compared to

the younger stars which have metallicities more uniformly distributed from -2 to 0.5 due to fresh material falling into the bulge, whereas the older stellar population was likely formed in ISM enriched by a supernova in the early life of the Milky Way's bulge.

The used bulge profile for modelling the central spheroidal component of galaxy is profile:

$$\sum_{bulge}(R) = \sum_0 \exp(-\beta[(\frac{R}{R_{bulge}})^{1/4} - 1]) \quad (11)$$

where \sum_0 is the surface mass density at the scale radius R_{bulge} , and $\beta = 7.695$. Then the total bulge mass is given by:

$$M_{bulge} = 2\pi \int_0^{+\infty} R \sum_{bulge}(R) dR \quad (12)$$

The bulge contribution to the circular velocity is computed as:

$$V_{bulge}^2 = \frac{GM_{bulge}}{R} \quad (13)$$

4.4 Halo

The galactic halo refers to the approximately spherical component of a galaxy that extends beyond the more dense, luminous component. It is composed of the stellar halo, the galactic corona and the dark matter halo.

4.4.1 Cuspy Dark Matter Halo

A dark matter halo in cosmological simulations of cold and collisionless dark matter has a density profile that rises toward the center with a power index of -1 to -1.5 referred to as a cuspy profile. The ΛCDM is the cosmological model that has had tremendous success in understanding the cosmic structure across time on large scales, but this model is being challenged by observations on same problem, the missing dwarf problem, and the missing dwarf problem. To understand the cuspy dark matter halo the observations of dark matter density profile must be done in various local galaxies. These shapes of Dark Matter halos in galaxies and clusters are fitted by empirical formulae. A radial density profile parametrization is

$$\rho DM(r) = \rho_0 / [(\frac{r}{r_s})^\alpha (1 + (\frac{r}{r_s})^{3-\alpha})], \quad (14)$$

where ρ_0 is a normalization constant and $0 \leq \alpha \leq \frac{3}{2}$.

4.4.2 Cored Dark Matter Halo

There are two main mechanism that cause expansion in dark matter; Supernova feedback and dynamical friction. Supernova feedback drives sufficient gas outflows to flatten the central Dark Matter density profile in simulated dwarf galaxies into a 'core'. Dynamical friction soothes dark matter density profiles during merges. A galaxy retains a cored profile at higher stellar-to-halo mass ratios, supernova feedback drives the expansion of the dark matter and generates cored profiles. For the cored profile consider the Einasto profile parametrization

$$\rho_{DM}(r) = \rho_e \exp -d_n[(\frac{r}{r_e})^{\frac{1}{n}} - 1], \quad (15)$$

where the term d_n is a function of n such that ρ_e is the density at r_e , which defines a volume containing half of the total mass. At $r = 0$ the density profile is then finite and cored. Another profile is the Burkert profile, which is an empirical law that resembles a pseudo-isothermal halo. It has a central core and is characterised by the core radius r_s and the central density ρ_0 .

$$\rho_{DM}(r) = \rho_0 / [(1 + \frac{r}{r_s})(1 + (\frac{r}{r_s})^2)], \quad (16)$$

The Burkert profile has a constant core density which fitted dwarf galaxy halos well in 1995, but no longer does so.

The circular velocity of the above dark matter profiles can be written as:

$$V_{DM}^2 = \frac{GM_{DM}(< R)}{R} \quad (17)$$

4.5 Modelling a mock rotation curve

I modelled the Rotation curve galaxy which has stars, HI gas and Dark Matter halo. The galaxy has the following properties:

Component	Value
Stellar mass (MD)	$3 \times 10^{10} M_\odot$
Stellar disc radius (RD)	$2 kpc$
HI gas Mass	$10^9 M_\odot$
Gaseous disc radius	$3 \times RD(kpc)$
DM Core radius	$5 kpc$
DM core density	$1 \times 10^{-23} \frac{gm}{cm^3}$

the model goes from radius of 0.01 to 20 kpc see model 17. I used python to compute the velocity profiles according to section 4 and python matplotlib library to produce the rotation curve.

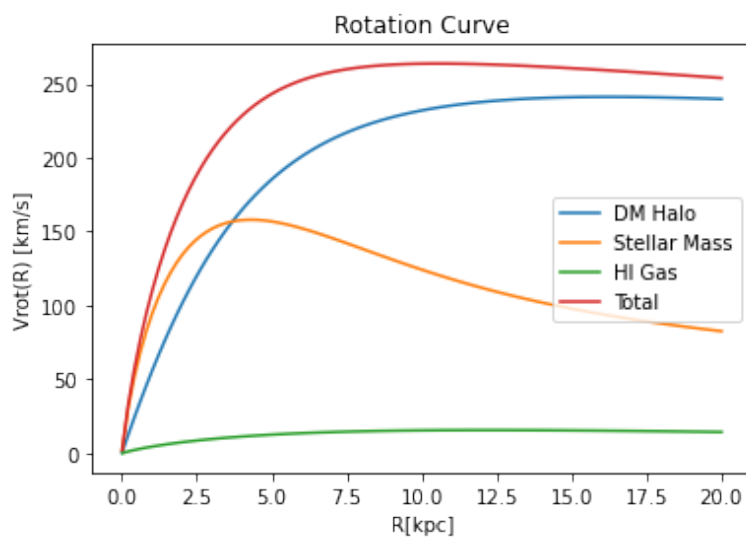


Figure 17: Modelled rotation curve: I am plotting circular velocity of various components of modelled galaxy as function of its radius. Where the red curve shows the total contribution to circular velocity, the blue curve shows the dark matter circular velocity and the orange and green showing for the stars and HI gas respectively.

5 Results

5.1 Testing Barolo

In this section, we are evaluating, qualitatively and quantitatively, the situation when a galaxy parameter is fed wrong in Barolo run. In particular, we study barolo moment maps and position velocity diagram due to wrong Position Angle, Inclination Angle and Systematic Velocity. Qualitatively: we visualize images, and Quantitatively: we estimate the relative error. Relative error is defined as the ratio of the absolute error of a measurement to the measurement being taken. We will use it as a measure of precision, expressed as a percentage. Formula:

$$RE = \left| \frac{V_{true} - V_{estimate}}{V_{estimate}} \right| \times 100$$

5.1.1 Position Angle

Changing the position angle by $(-20, +20)$

Position Angle		
Lower	True	Upper
103, 7°	123, 7°	143, 7°

A table of relative error of rotational velocity due to the change in Position angle

Value	Velocity	Relative error
Lower	99.99	14.11
True	121.21	2.23
Upper	100.61	11.91

5.1.1.1 Moment Maps

Visualizing the moment maps of the different PA's.

When the position angle value is lowered we can see that it lowers the tilt or it rotates the map clockwise with reference to the true angle. When the position angle value is increased then this gives an anti-clockwise rotation of the maps with reference to the true angle. In the First Moment (Intensity) the true PA shows high concentration of surface brightness at the centre however this changes when the PA is lowered or increased where the intensity is widely spread throughout the map with decreasing values from the center. The changing of PA from increases the residuals, we can see that the residuals are low around the center along the major axis and are very high at the edges of the map.

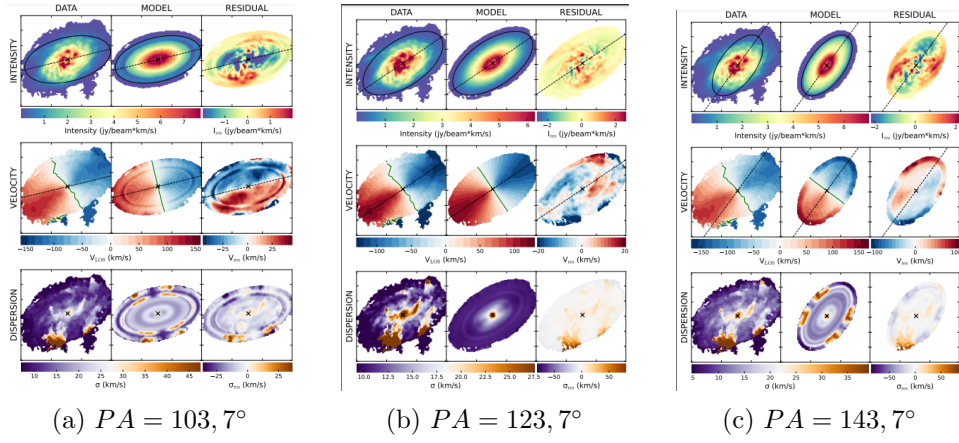


Figure 18: Moment maps of NGC2403 for different Position angle

In the Second Moment (Rotational Velocity), the true PA shows (dark blue and red colour) high values of blue and red shift and this changes with the lowering and increment in PA as the colours turn to be lighter which implies a decrease in the velocities of the blue and red shift. For this moment, the residuals have low values for lower PA in compared to upper PA. When PA is increased, the residuals show high velocity values at the edges following the same pattern for blue and red shift. For lowered PA, there is high blue shift velocities over the major axis and high red shift velocities below the major axis.

In the 3rd moment (velocity dispersion), the true PA shows high values near the center on third quadrant of the minor and major axis, same behaviour for the lowered and increased PA maps, But the model for this Moment shows medium value spread of the dispersion velocity when you move away from the center. The residuals follow the pattern of the other moments, i.e., a dramatic increase in the residuals due to the change in PA. In this moment, we observe high values for lowered PA in compared to increased PA.

5.1.1.2 P-V diagram

The diagram consists of P-V Diagram consists of two diagrams, namely the top rotational curve and the bottom Vertical PV diagram. Looking into the rotational curve, the yellow squares gives the best measurement of the Line of Sight velocity, the red contours represent the model and the blue contour represent the data. These contours overlap for for the True PA and they do not overlap for the lowered and increased PA values. Following the yellow squares, for the true PA we have a perfect fit in compared to the depiction obtained when the PA was lowered and increased. The best fit curve follows the same trend for all the different PA. V_{los} increases exponentially from the

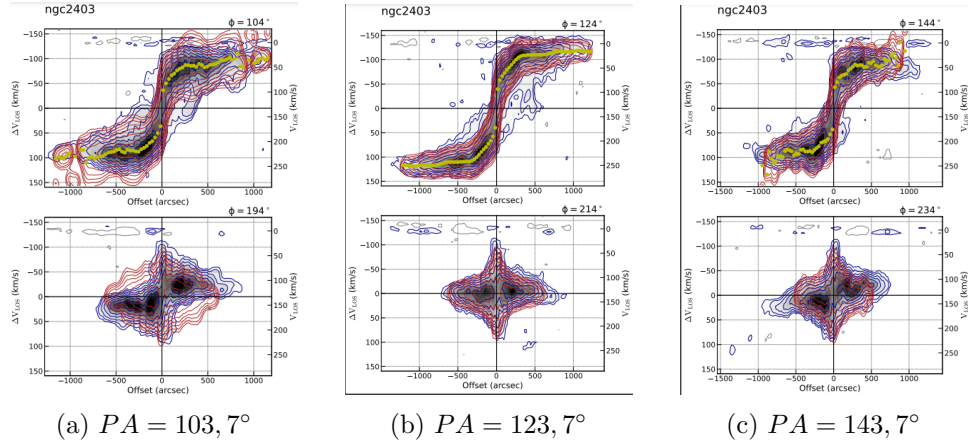


Figure 19: P-V Diagram of NGC2403 for different Position angle

center as the curve picks an exponential form and becomes almost constant the further it is from the center/origin. The best fit parameter for the lowered PA shows imperfections and inconsistency in the curve as it moves away from the origin. The increased PA best fit parameter curve is not looking good, its irregular throughout the trend.

Notice that the vertical PV diagram for true PA is very symmetric around the axis, while for the increased and lowered PA, its asymmetric. The red contour (model) and blue contour (blue) overlap for the true PA value but no overlap for the lowered and increased PA value.

5.1.2 Inclination Angle

Changing the inclination angle by $(-40, +40)$)

Inclination Angle		
Lower	True	Upper
20°	60°	100°

A table of relative error of rotational velocity due to the change in Inclination Angle

Value	Velocity	Relative error
Lower	155.88	3.62
True	121.21	2.23
Upper	110.25	4.37

5.1.2.1 Moment Maps

The change in Inclination shows a change in the thickness of a galaxy. Decreasing the Inclination angle thickens the map as it enlarges the minor axis

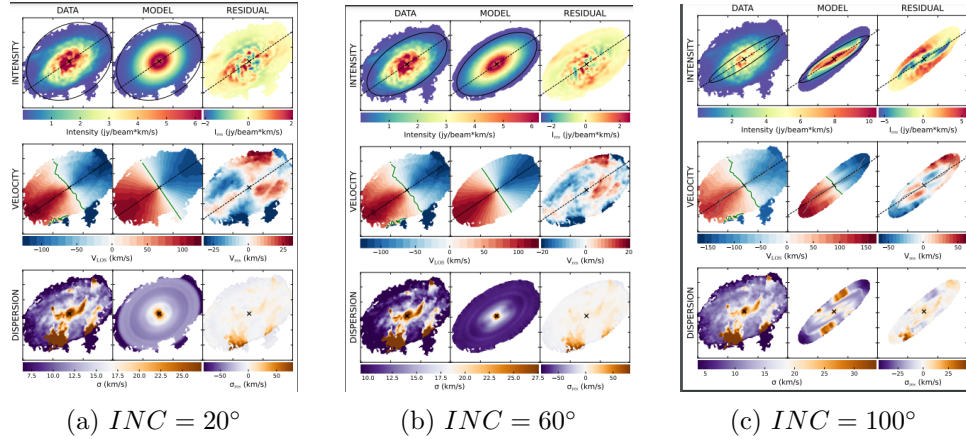


Figure 20: Moment maps of NGC2403 for different Inclination Angle

whereas increasing the Inclination angle decreases the minor axis. In the first moment for true INC the data and model show an exponential brightness profile as the intensity values are very high at the center and decreases exponentially as you move away from the center. For the lowered INC the intensity still follows the same exponential profile, the only difference is the enlarged minor axis, but for the increased PA value, the data does not show very high intensity values around the center but the model shows very high values because it shows red colour in accordance to the scale bar its for high intensity. The residuals for the true INC and lowered INC are the same but different for upper INC, the residuals show higher values around the edges of the galaxy.

In the second moment the map shows almost the same velocity maps for the true and lowered INC values, the blue and red shift velocity values ranging from 100 km/s but, for the increased value, the the map shows low blue and red shift velocities for the data but high values around the edges along the major axis for the modelled map. The residuals share the same nature depiction for lowered and true INC value where the map shows high blue shift values below the major axis and high red shift values above the major axis. The increased INC residuals also follow the same trend of high blue and red shift values around the edges below the major axis and above the major axis respectively.

In the third moment, the data maps show the same trend on the values of the velocity dispersion but higher values for the lowered and true INC values. The model map is different across all the different INC values. We see a symmetrical distribution of the velocity dispersion, high values in the center but uniform mid value for velocity dispersion from the centre until the edges where very low values are shown. The same happens for the true value, but only high value at the center and a uniform distribution of low

velocity dispersion values from the center as the map is covered in blue. For the increased value the model depicts a very thin map of random distribution of velocity dispersion values. The residuals follow the same trend, just a thin map for the increased INC.

5.1.2.2 P-V diagram

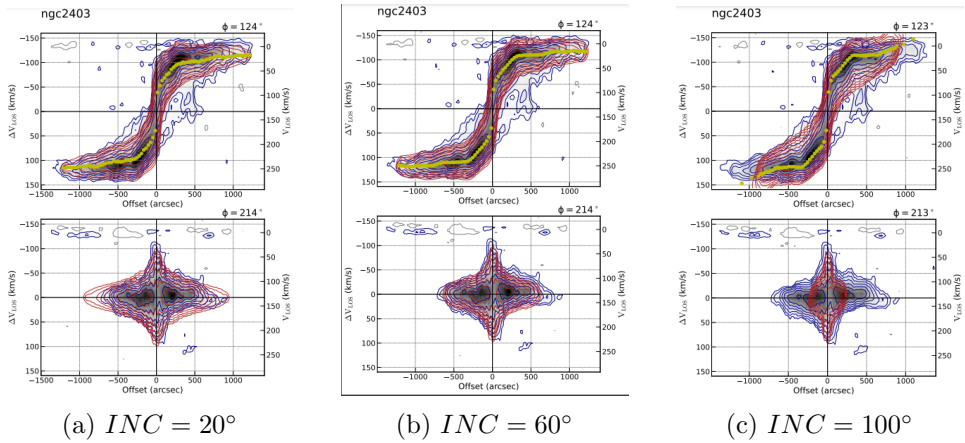


Figure 21: P-V Diagram of NGC2403 for different inclination angle

Looking into the rotational curve, the yellow squares give the best measurement, these follow the same trend where we observe almost the same values. The contours overlap for the True INC and overlap for the lowered and increased INC values. Following the yellow squares, for the true INC we have a perfect fit in however, the increased and lowered INC do not have much effect on the curve as the curves are similar throughout the different INC values. The best fit curve follows the same trend for all the different INC. V_{los} increases exponentially from the center as the curve picks an exponential form and becomes almost constant the further it is from the center/origin.

The vertical PV diagram for true INC is very symmetric around the axis, however, this is also true for the INC false values. The change in INC rather has no huge effect on V_{los} .

5.1.3 Systematic Velocity

Changing the Systematic Velocity by $(-50, +50)$)

Systematic Velocity		
Lower	True	Upper
82,8 km/s	132,8 km/s	182,8 km/s

A table of relative error on rotational velocity due to the change in Systematic Velocity.

Value	Velocity	Relative error
Lower	181.56	5.38
True	121.21	2.23
Upper	184.63	5.90

5.1.3.1 Moment Maps

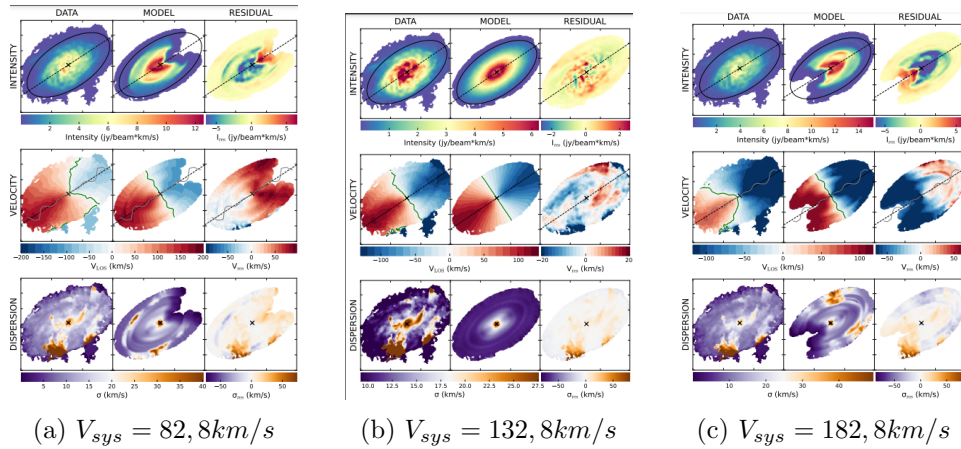


Figure 22: Moment maps of NGC2403 for different Systematic Velocity

The impact of changing the systematic velocity has a lot of impact on the moments. For the lowered Systematic Velocity, consider the First Moment (Intensity), a lot of intensity at the center and decreasing as you move away from the centre, there is no high concentration of surface brightness at the center for the data however the model contains rather a different image compared to the observed intensity, where the intensity follows the exponential profile. High values of residuals observed at the center and decreasing with extension of the map from the center. For the increased Vsyst the intensity follows the description and behaviour of the lowered Vsyst. In the Second Moment (Vrot) with a lowered Vsyst, the blue and red occur at low velocities as we see light red and blue. For the increased Vsyst the blue and red shift occur at very high velocities as we observe dark blue and red colours in the maps. In the third moment (Vdisp), there change in the lowering and increment of Vsyst is the same as we see that there is high values of Vdisp by the edge/circumference on the left bottom side of the major axis. Throughout all the moments we observe a spot of zero intensity, Vrot, Vdisp by the right top side of the major axis when Vsyst is lowered and this occurs in the opposite side of the major axis when Vsyst is increased. Perfect fit is only observed at fixed Vsyst.

5.1.3.2 P-V diagram

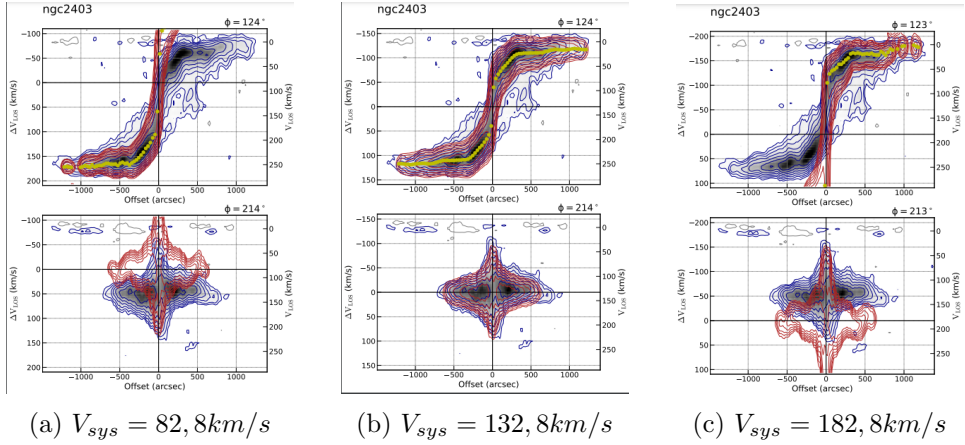


Figure 23: P-V Diagram of NGC2403 for different systematic velocity

Interesting changes observed in the P-V diagram, for the lowered Vsyst we have no best parameter values in the 1st quadrant, we observe the blue contours/lines which show the data values but there are no red contours which means that there's is failure in fitting the model for low Vsyst values but there are values in the 3rd quadrant. We observe the opposite behaviour when Vsyst is increased, the best fit is only curve only shows in the first quadrant and nothing in the 3rd quadrant.

In the vertical PV diagram, we can see the model contours lying above the data which confirms what's shown in the curve, the model fits the velocity of the negative direction for the lowered Vsyst and the opposite occurs for the increased Vsyst, the model contours lie below the data contours confirming the positive fitted velocity values on the curve.

5.2 Dark Matter Fractions of NGC2403

In this section I will plot the rotation curve of NGC2403 which I derived through Barolo. In figure 24, we have the rotation curve of NGC2403 derived from 3D Barolo. This is a rotation curve expands to radii of 20 kpc having maximum velocity of $132, 8 \text{ km/s}$, from section 3.2, the galaxy has stellar disc length: 2 kpc , HI disc scale length: 20 kpc , stellar mass: $3 \times 10^{10} M_\odot$, molecular gas mass: $10^9 M_\odot$, effective radii: 7 kpc . Using this information I modelled the Rotation curve of NGC2403.

In figure 25 we have the modelled rotation curve given the stellar mass and HI gas mass in section 3.2: I computed stellar and HI gas velocities. Finally computed baryonic matter velocity where $V_{bar} = \sqrt{V_{star}^2 + V_{gas}^2}$

I decomposed the baryonic component from the total observed velocity of the galaxy and computed the dark matter fractions using the following

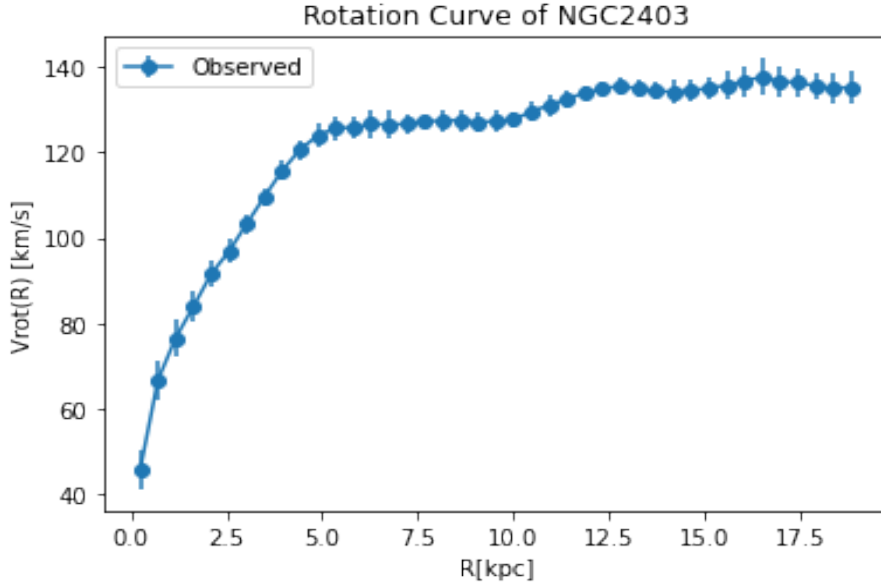


Figure 24: Barolo derived rotation curve, plot of the observed rotational velocity of NGC2403

formula:

$$f_{DM} = 1 - \frac{V_{bar}^2}{V_{obs}^2} \quad (18)$$

Looking into figure 26, it shows that in the inner region of the galaxy we have about 40% of dark matter fractions which decreases as you approach the effective radius and starts increasing after this point. In comparison to figure 25, the inner region is dominated by baryonic matter since the V_{rot} for baryonic matter increases to high values until the effective radius. The observed V_{rot} and baryons V_{rot} both increase from the center however after the effective radius, the observed V_{rot} remains about constant whereas the baryons V_{rot} decreases after the point of effective radius. To cover for the difference between the observed and baryonic rotational velocities, we see the increase in dark matter fractions after effective radius. Our galaxy NGC2403 is a baryonic matter dominated galaxy at the inner region and is dark matter dominated at the out-skirts which covers the halo. The dark matter fractions go up to 60% which proves that NGC2403 has a dark matter dominated halo.

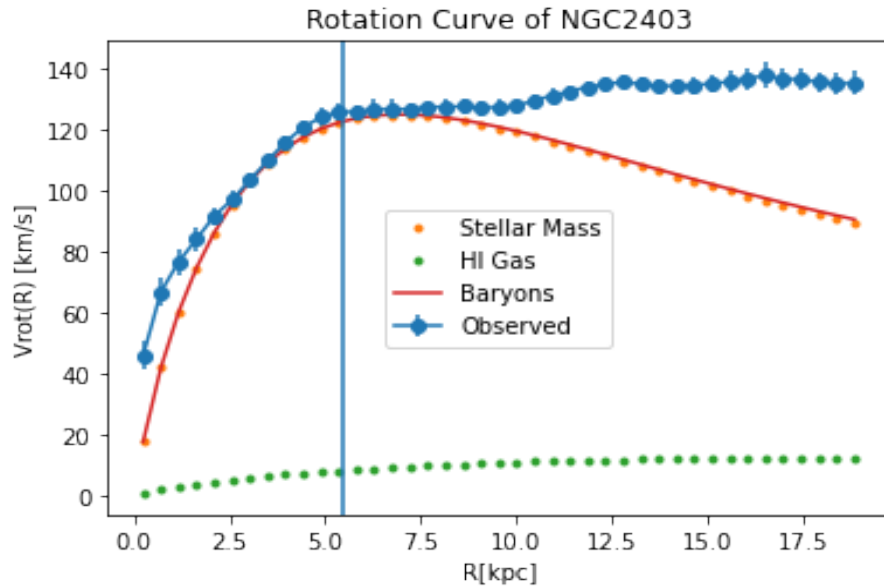


Figure 25: Modelled rotation curve of NGC2403, I am plotting circular velocity of the various components of NGC2403 as a function of radius, where, the blue curve shows the observed circular velocity, the dotted orange and green shows the circular velocity of stars and HI gas respectively and lastly the red curve shows the baryonic matter circular velocity of NGC2403

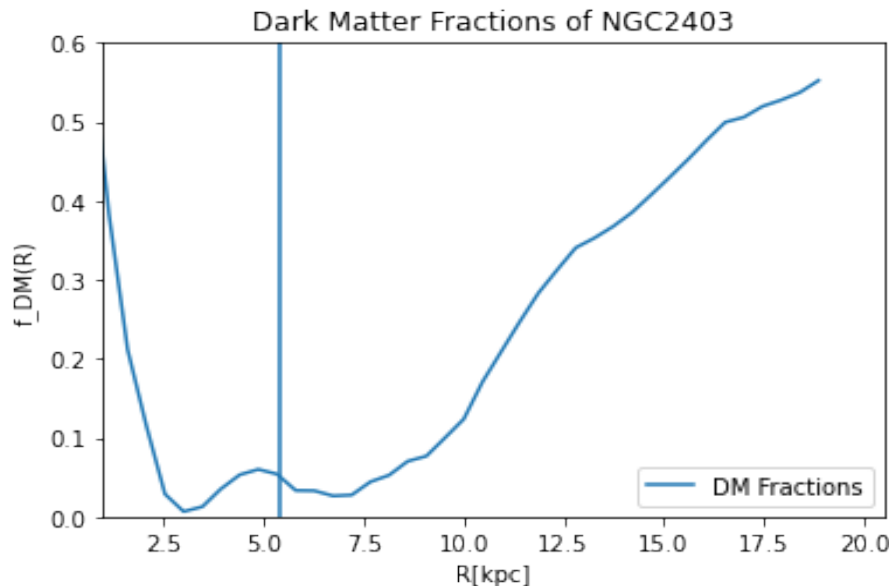


Figure 26: Dark Matter Fractions of NGC2403

6 Conclusion

The project has been informative. I have learned about galaxy kinematics and dynamics. The relation of rotational velocity and the mass distribution plays a huge role in determining dark matter content in a galaxy. Firstly, I learned and used Barolo to derive the kinematics of galaxy NGC2403. I enhanced my python programming skills as I had to display the outputs using python. I had to learn and understand the outputs namely, Moment maps, Channel maps, P-V diagram and ring files. I tested Barolo and the results are obtained in section 5. Furthermore, I performed relative error analysis on the testing output values and the error of the true value was lower compared to the changed values, this was done using python. Finally, I produced the modelled rotation curve and visualized the results using python and thereafter computed dark matter fractions and plotted the results. This all has allowed me to study the dark matter content of NGC2403, which means that I have met my initial aim of the project to determine dark matter content of NGC2403.

Dynamical mass modelling of NGC2403, shows that the dark matter fraction in the inner region (< 0.5 kpc) is $\sim 50\%$, and it gradually decreases between ($1 - 2.5$ kpc). In the baryon dominated region, that is where stars and gas dominates, the dark matter fraction is $\sim 5-10\%$. In the outskirts, > 7.5 kpc, dark matter fraction gradually increases. In the most flattest region of rotation curve, dark matter fraction is about $\sim 60\%$, that is dark matter is dominating. This suggest that galaxy have a dark matter halo around it which extends much further than its visible matter. The increase of dark matter fraction in the inner region suggests that the dark matter is likely having a high-density core, which I plan to investigate in future.

I learned that there is still a lot to learn about galaxy dynamics and their dark matter content. Therefore, in future, I plan to do my masters project focused on galaxy dynamics and their dark matter content where I will be guided to reduce and analyse the state-of-the-art galaxy observations of radio and optical wavelength. Thereafter, I will derive the galaxy kinematics and dynamics of large datasets, scaling relations of galaxy properties, and structural properties of dark matter.

References

- [1] Bulges.
- [2] Deep hi survey of the spiral galaxy ngc 2403.
- [3] What are elliptical galaxies, Jan 2019.
- [4] Daniel Clery. Black holes caught in the act of swallowing stars. *Science*, 367(6477):495–495, January 2020.
- [5] Malcolm S Longair. The simplest picture of galaxy formation and why it fails. In *Galaxy Formation*, pages 274–292. Springer, 1998.
- [6] Mario Mateo. Dwarf galaxies of the local group. *arXiv preprint astro-ph/9810070*, 1998.
- [7] JI Read, AP Pontzen, and Matteo Viel. On the formation of dwarf galaxies and stellar haloes. *Monthly Notices of the Royal Astronomical Society*, 371(2):885–897, 2006.
- [8] Gauri Sharma et al. Nature of dark matter from the astrophysics of high redshift star-forming galaxies. 2021.
- [9] Hsiang-Hsu Wang. *Gas Evolution in Disk Galaxies*. PhD thesis, Ph. D. Thesis. Faculties of the Natural Sciences and Mathematics, University . . . , 2010.